Efects of biogas combustion with oxygen-enriched air in a spark-ignition internal combustion engine

James G. Pereira[a] and Waldyr L. R. Gallo[b]

[a] *University of Campinas, Campinas, Brazil, james.gomes1397@gmail.com*
[b] *University of Campinas, Campinas, Brazil, gallo@fem.unicamp.br*

Abstract:
The development of internal combustion engines (ICE) represents one of humanity's greatest technological advances, having significantly boosted the power generation, energy, and propulsion sectors. Due to the growing need to mitigate greenhouse gas emissions from fossil fuels, new technologies and the use of alternative fuels is increasing importance and ensure that these engines still have a long-lasting future. In this context, biogas, resulting from the anaerobic decomposition of organic matter and composed mainly of methane (CH_4) and carbon dioxide (CO_2), emerges as a promising alternative. However, the use of biogas imposes several performance losses to the engine. This work aims to evaluate, through a quasi-dimensional two-zone simulation model, the effects of using biogas in a stationary spark ignition engine using oxygen-enriched air to recover engine performance. The oxygen is supposed to come from hydrogen production through electrolysis. This option still faces challenges, requiring computational studies capable of adequately representing the phenomena of turbulent combustion in ICEs with oxygen-enriched air. The model incorporates a thermodynamic module coupled to a turbulent combustion model, used to determine the profile of the burned mass fraction based on the turbulent flame velocity. The laminar flame speed was calculated with Cantera software using the *GRI-Mech 3.0_highT* kinetic mechanism, considering a mixture of 60% CH_4 and 40% CO_2 by volume and different concentrations of oxygen in the intake air (21% to 30% v/v). The effect of oxygen enrichment on the flame speed was identified. The MBT spark condition was determined for each operating point. The variation of the compression ratio (12:1 to 16:1) was evaluated, as well as the intake pressure increase. The results shown that the use of a compressor or turbocharger to increase intake pressure is the most promising strategy, resulting in significant performance gains and an increase of more than 40% in volumetric efficiency, with no evidence of detonation risk.

Keywords:
Internal combustion engines, Biogas, Oxygen-enriched air, Turbulent combustion.

1. Introduction

Internal combustion engines (ICEs) are widely used, particularly in the transport and power generation sectors. Due to certain characteristics, such as their simplicity, robustness and high power-to-weight ratio, these engines remain the primary solution for freight transport, marine transport, agricultural machinery and power generation. However, when operating on fossil fuels, ICEs play a central role in the challenge of climate change, as they contribute significantly to greenhouse gas (GHG) emissions and air pollutants.

In the face of accelerating climate change, electric vehicles (EVs) have emerged as a crucial solution. However, this transition faces significant challenges, not only regarding the technological development of EVs, but also regarding the true environmental impacts associated with the use of this new technology. [1] argue that life-cycle analyses of the GHG impact of EVs show that their true benefit is significantly lower than it appears at first glance. Furthermore, a growing fleet of EVs represents a potentially substantial shift in demand from fossil fuels to electricity. EVs will account for over 15%

of total growth in electricity demand by 2050 and have become one of the main drivers of electricity demand [2].
According to [1], there are still no viable alternatives that can compete with the internal combustion engine across the full range of applications it covers. Consequently, the internal combustion engine will continue to play a central role, whether used for power generation or to power the vehicle itself. Research conducted by [3] estimates that approximately 80% of vehicles sold by 2050 will still be equipped with internal combustion engines, including naturally aspirated spark ignition (NASI), turbocharged spark ignition (TCSI) and diesel engines. Therefore, the approach to reducing GHG emissions in the transport and electricity generation sectors must be multifaceted, taking into account both the transition to electric vehicles and other technologies, such as the use of biofuels in ICEs.
Biogas is a mixture of gases produced by the anaerobic decomposition of organic material, predominantly generated in biodigesters and landfill sites, consisting mainly of methane (CH_4) and CO_2. However, [4] states that the composition of raw biogas can be influenced by various factors, such as the substrate and the fermentation technology used in production, resulting in the presence of small quantities of other elements, namely hydrogen sulphide (H_2S), hydrogen (H_2), nitrogen (N_2), ammonia (NH_3), oxygen (O_2) and carbon monoxide (CO). Furthermore, biogas is saturated with water and also contains dust particles, siloxanes, aromatic and halogenated compounds.
According to [5], in recent years, the anaerobic digestion of agricultural and industrial waste, municipal organic waste and sewage sludge has become one of the most promising avenues for the energy transition.
In this context, the suitability of biogas for use in internal combustion engines makes it one of the leading alternative fuels. However, studies such as those in [6] and [7] on the combustion and use of CH_4 and CO_2 mixtures in internal combustion engines have shown that the high CO_2 content in biogas reduces engine performance parameters. The presence of CO_2 reduces the calorific value of biogas, the adiabatic flame temperature and the burn rate, and consequently the combustion efficiency. Study [7] further states that the effects of the high CO_2 content on the combustion parameters of biogas used in ICEs can be mitigated by enriching the air with oxygen (O_2).
Hydrogen is widely recognised as one of the most promising energy carriers for future sustainable energy systems, and new projects on various scales are being developed globally for its production. However, as stated in the study [8], the electrolysis process generates not only hydrogen but also approximately eight times as much oxygen by mass. Thus, the production of large volumes of hydrogen inevitably involves the generation of oxygen as a by-product on a large scale.
Hydrogen and oxygen, obtained as by-products, can be utilised simultaneously in various processes. Combustion air enriched with oxygen offers great potential for application in gas turbines (GT) and stationary engines in power generation plants. Hydrogen, in turn, can be utilised in applications such as fuel cell vehicles (FCVs) and in combined heat and power generation.
The experimental results of a study [9], conducted on a stationary compression-ignition engine operating in a dual-fuel mode (diesel-biogas) using a typical biogas composition of 60% CH_4 and 40% CO_2 by volume, indicated a significant reduction in fuel ignition delay, as well as an increase in pressure values and thermal efficiency. The oxygen concentration in the engine's intake air ranged from 21% to 27% by volume.

2. Methodology

The predictive model used in this study is based on a phenomenological model initially developed by [10]. The author developed a two-zone thermodynamic model and utilised the models proposed by [11] and [12] to describe the heat transfer process in the closed and open phases, respectively. The combustion process was modelled using the Wiebe function, and the combustion parameters were obtained from experimental data provided by the Mauá Institute of Technology (IMT). In this study, the phenomenological model was converted into a quasi-dimensional model through the implementation of a turbulent combustion model. The predictive model was able to predict combustion parameters

for different fuels, as well as engine performance parameters.
The predictive model was applied to simulate a conventional engine running on biogas, the composition of which was set at 60% CH_4 and 40% CO_2. The oxygen concentration in the intake air varies between 21% and 30%; the input data used in the simulation are presented in Table 1.

Table 1: Input data for the simulation model.

Parameter	Value	Unit
Atmospheric pressure (P_0)	95e3	Pa
Ambient temperature (T_0)	295	K
Compression ratio (TC)	12:1	-
Cylinder diameter (d)	68	mm
Connecting rod length (l)	145	mm
Piston stroke (L)	110	mm
Intake valve diameter (d_{va})	30.93	mm
Exhaust valve diameter (d_{ve})	28.27	mm
Angular duration of the intake valve lift (θ_{va})	230	degrees
Angular duration of the exhaust valve lift (θ_{ve})	245	degrees
Maximum lift of the intake and exhaust valves ($Y_{D_{max}}$)	0.3	-
Intake valve lift start angle	700	degrees
Exhaust valve lift start angle	490	degrees
Temperature of the cylinder walls (T_w)	520	K
Theoretical air coefficient (λ)	1	-
Lower calorific value of the fuel (PCI)	17	MJ

2.1. Two-zone phenomenological model

This model is considered only in the closed phases, since in the open phases there is only the region of unburned gases. The hypotheses adopted to implement the phenomenological model are as follows:

- Both zones are in mechanical equilibrium, i.e. the same pressure;
- Gas leakage through the ring gap into the crankcase (blow-by) was disregarded;
- Burnt and unburnt gases do not mix;
- The zones are separated by the flame front;
- The flame is considered impermeable and adiabatic and has an infinitesimal width;
- Heat transfer from the cylinder walls to the cooling water is not modeled. The cylinder walls are considered to be at constant temperature;
- Heat transfer is considered to occur exclusively by convection. Radiation is disregarded.

The development of the two-zone model is based on assuming that the cylinder charge during combustion is divided into two zones: the combustion products and the unburned reactants. As combustion takes place, a zone of burned gases develops, while the zone of unburned gases is reduced, as shown in Fig 1.
From the energy balances of the burned and unburned zones and the volume differentials, the differential equations for the temperature of the burned gases T_b, the temperature of the unburned gases T_u and the pressure P are obtained, according to (1), (2) and (3). The complete development of the equations is provided by [10].

$$\frac{dT_b}{d\theta} = \frac{\frac{dH_{comb}}{d\theta} + \frac{dQ_b}{d\theta} + \frac{dm_b}{d\theta}\left(c_{p,u}T_u - c_{p,b}T_b\right) + V_b\frac{dP}{d\theta}}{m_b c_{p,b}} \tag{1}$$

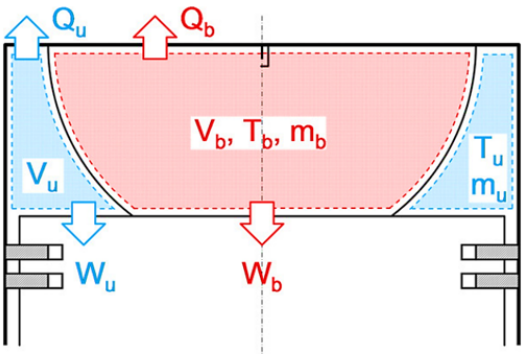

Figure 1: System considered for the two-zone model. Adapted from: [13]

$$\frac{dT_u}{d\theta} = \frac{\frac{dQ_u}{d\theta} + V_u \frac{dP}{d\theta}}{m_u c_{p,u}} \tag{2}$$

$$\frac{dP}{d\theta} = \frac{P\frac{dV}{d\theta} - R_u T_u \frac{dm_u}{d\theta} - R_b T_b \frac{dm_b}{d\theta} - \frac{R_u \frac{dQ_u}{d\theta}}{c_{p,u}} - \frac{R_b \frac{dH_{comb}}{d\theta} + \frac{dQ_b}{d\theta} + \frac{dm_b}{d\theta}\left(c_{p,u}T_u - c_{p,b}T_b\right)}{c_{p,b}}}{\frac{V_b R_b}{c_{p,b}} + \frac{V_u R_u}{c_{p,u}} - V} \tag{3}$$

In (1), (2) and (3), m_b, m_u, V_b and V_u represent the masses of the burned and unburned gases, respectively, and the corresponding volumes. The terms R_b, R_u, $c_{p,b}$ and $c_{p,u}$ represent, respectively, the constants of the burned and unburned gases and their respective specific heats at constant pressure.
The pressures reached in engines are quite high, especially in the combustion process. However, [14] states that the ideal gas assumption in the thermodynamic modelling of the process is quite reasonable. In this work, the thermodynamic property values were obtained on a molar basis by 6th order temperature polynomial functions adjusted by [15] using data from the JANAF tables.
The heat transfer rate, represented by the term $\frac{dQ}{d\theta}$, is assumed to result mainly from convection between the gases and the cylinder walls, given that radiation plays a minor role in spark-ignition engines, as shown in the studies in [16] and [17]. Therefore, the heat transfer rate is obtained from (4), which depends on the instantaneous heat transfer area A and the estimated temperature of the cylinder walls T_w. The heat transfer coefficient h^{HT} is obtained from the Hohenberg correlation as a function of pressure, temperature, volume and piston speed v_m, as shown in (5).

$$\frac{dQ}{d\theta} = -\frac{h^{HT} A (T - T_w)}{\omega} \tag{4}$$

$$h^{HT} = 130 V^{-0.06} P^{0.8} T^{-0.4} (v_m + 1,4)^{0.8} \tag{5}$$

The rate of energy released by the combustion process, represented by the term $\frac{dH_{comb}}{d\theta}$, is proportional to the burning rate $\frac{dx_b}{d\theta}$ and can be calculated as a function of the mass of fuel admitted m_{comb} and the enthalpy of combustion h_{comb}, as shown in (6).

$$\frac{dH_{comb}}{d\theta} = \eta_{comb} m_{comb} h_{comb} \frac{dx_b}{d_\theta} \tag{6}$$

The term η_{comb} is called combustion efficiency and can be defined as a function of the theoretical air coefficient λ and the maximum combustion efficiency $\eta_{comb,max}$. Combustion efficiency is associated with the amount of energy converted into thermal energy in the combustion process and can be given by (7).

$$\eta_{comb} = \eta_{comb,max}(-1.6082 + 4.6509\lambda - 2.0764\lambda^2) \tag{7}$$

2.2. Combustion modeling

The combustion model used in this work is based on the considerations originally postulated by [18] of a combustion process involving the turbulent entrainment of the unburned mixture. [19] argue that this model divides the combustion process into two stages: first, the unburned mixture is entrained into the flame with a characteristic entrainment speed, and then the burning of the entrained eddies takes place. As is well known, the fluid flow in the combustion chamber is, for the most part, turbulent, and turbulence significantly influences the combustion process, as observed in the experimental studies in [20]. Thus, the burning of the charge inside the cylinder is considered a turbulent flame propagation process. Throughout this process, the unburned eddies of radius l_t are entrained into the flame zone at the entrainment speed U_e (which is considered to be the sum of the characteristic speed U_t and the laminar flame speed S_l of the unburned mixture) and then burned at the laminar flame velocity S_l in a characteristic time $\tau_b = l_t/S_l$, as described in study [21] and shown in Fig 2. The combustion model is described by ordinary differential equations, according to (8) and (9).

$$\dot{m}_e = \rho_u A_f (U_t + S_l) \tag{8}$$

$$\dot{m}_b = \rho_u A_f S_l + \frac{(m_e - m_b)}{\tau_b} \tag{9}$$

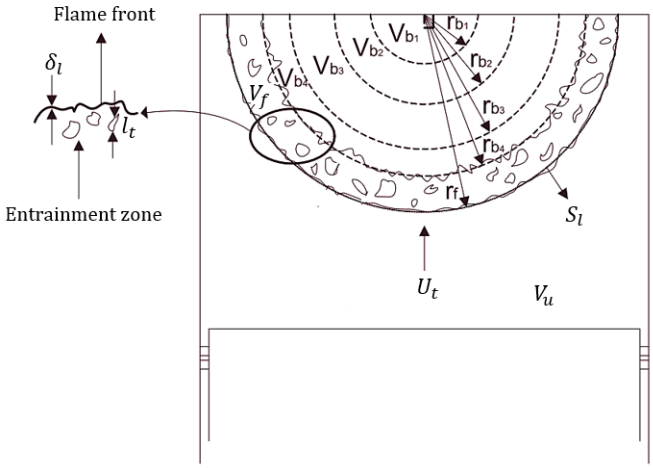

Figure 2: Schematic of the entrainment combustion model. Adapted from: [19]

The thermodynamic properties used in the (8) and (9) are provided from the two-zone phenomenological model mentioned above. The application of this combustion model follows the following assumptions, essentially based on experimental observations made by various authors [18], [19] e [20]. During the first stage of combustion, referring to the fuel ignition delay, the flame front expansion speed is close to that of a laminar flame, so combustion is considered laminar ($U_t = 0$ and $m_e = m_b$). After this period, the main stage of combustion begins and the flame becomes turbulent. In this case, the instantaneous values of U_t and l_t are determined using the following correlations, based on the application of (10) and (11) to various combustion data sets in engines, as stated in the study [22].

$$U_t = 0.08\bar{u}_i \left(\frac{\rho_u}{\rho_i}\right)^{1/2} \tag{10}$$

$$l_t = 0.8 L_{iv} \left(\frac{\rho_i}{\rho_u}\right)^{3/4} \tag{11}$$

The terms $\bar{u}_i$, L_{iv} and ρ_i represent the average velocity of the inlet gas, the maximum lift of the inlet valve and the density of the mixture evaluated in the reference state. [23] propose a correlation for $\bar{u}_i$

in terms of the volumetric efficiency η_v, the piston area A_p, the maximum intake valve opening area A_{iv} and the average piston speed v_m. This correlation is given by (12).

$$\bar{u}_i = \eta_v \left(\frac{A_p}{A_{iv}} \right) v_m \tag{12}$$

As suggested by [17], the (13) and (14), as a function of diameter D and the ratio between maximum lift and intake valve diameter Y_D, are used to calculate the area and maximum lift of the intake valve.

$$A_{iv} = 0.736311 D^2 \tag{13}$$

$$L_{iv} = D Y_D \tag{14}$$

Experimental studies, such as those in [18] and [20], have shown that combustion continues even after the entire cylinder charge has been swept into the flame front.. Therefore, at the end of flame propagation, even after the flame front has reached the walls of the combustion chamber, there is still a substantial amount of unburned mass. This stage of combustion is approximated by the following exponentially decreasing burning rate, as shown in (15).

$$\frac{dm_b}{d\theta} = \left(\frac{dm_b}{d\theta} \right)_F \exp\left(-\frac{\theta - \theta_F}{\tau_b} \right) \tag{15}$$

The terms $(dm_b/d\theta)_F$ and θ_F represent the mass burned and the angle, respectively, when the flame front reaches the walls of the combustion chamber.

To solve (8) and (9) of the turbulent entrainment combustion model, it is necessary to estimate the flame front area A_f and the laminar flame speed S_l during flame development. The flame front area is calculated from the geometric submodel described by [21] and [24], the details of which will not be presented here.

In this study, it is assumed that, during combustion in spark-ignition engines, the flame front propagates in the form of a sphere centred on the ignition point, as suggested by [22] and [24]. [21] proposes obtaining the flame front radius R_f from the volume of the flame region, given by (16).

$$V_f = V_b + \frac{m_e - m_b}{\rho_u} \tag{16}$$

The biogas flame speed data were determined using the open-source Cantera software package, which is widely used in the modelling and simulation of chemical and thermodynamic processes. The analysis was carried out based on an appropriate chemical kinetics model, taking into account the chemical composition of the fuel, the equivalence ratio, the temperature, the pressure and the excess O_2 present in the air. For this purpose, the *GRI-Mech 3.0_highT* chemical kinetics mechanism was adopted, which includes 325 reactions and 53 chemical species,according to the study in [25]. To reduce the computatiional cost of Cantera use, the flame velocity values obtained were fitted using (17) and (18) via the Levenberg–Marquardt method, as described in [26], implemented in the *curve_fit* function of the SciPy library in Python.

$$Sl(\phi, T_u, P) = Su_0(\phi) \left(\frac{T_u}{T_0} \right)^{\alpha} \left(\frac{P}{P_0} \right)^{\beta} \tag{17}$$

$$Su_0 = a\phi^2 + b\phi + c \tag{18}$$

Where T_0 and P_0 are, respectively, the reference temperature and pressure, and α and β are constants dependent on the fuel, the equivalence ratio and the diluent gas fraction. The reference laminar flame speed, Su_0, corresponds to the value of the flame speed for the reference conditions $T_u = T_0$ and $P = P_0$. The coefficients a, b and c are determined by curve fitting the values of the laminar flame

speed as a function of the equivalence ratio and the excess oxygen in the air, ranging from 21% (normal air) to 30% (oxygen enriched air).
The set of differential equations presented is solved by numerical integration, using a fifth-order Runge-Kutta method. The convergence of the model is verified by examining the difference between successive iterations of the pressure, temperature and mass variables, with an absolute error of less than 0.1% adopted as the criterion.

3. Results

This chapter presents and discusses the results obtained from simulations carried out using the algorithm described in the previous chapters. First, the proposed model is validated by comparing the simulated results with data available in the literature. Finally, a parametric study based on the excess oxygen is conducted to evaluate the influence of variations in ignition timing, rotational speed, compression ratio, and intake pressure, in order to verify the consistency of the algorithm's results with the trends expected based on the fundamentals of combustion and engine operation.

3.1. Comparison of the results obtained by the developed combustion model with those reported in the literature

The model was validated by comparing it with the results presented by [10]. In that study, the author simulated an engine with the same geometric characteristics, using ethanol hydrated with 5% water as fuel, and validated the results using experimental data provided by the Mauá Institute of Technology. In this study, the laminar flame speed of ethanol was determined using the Cantera software package, employing the ethanol.yaml kinetic model, which consists of 113 species and 710 reactions, as described in [27]. It should be noted, however, that although the model is easy to implement in the simulator, the associated computational cost is substantially high.

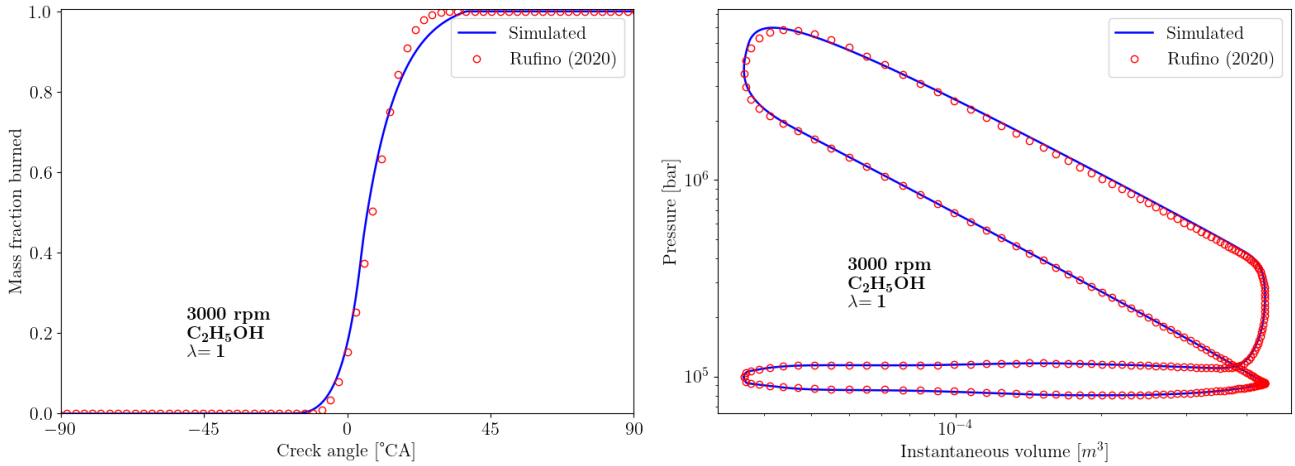

Figure 3: Comparison of mass fraction burn curves for ethanol.

As illustrated in Fig 3 a comparison of the results for the fraction of mass burned and instantaneous pressure obtained using the model developed in this study (the Keck model) with those reported in the model proposed by [10] shows a high degree of agreement. It is observed that the burned mass fraction curve calculated by the turbulent combustion model closely follows the curve estimated by the Wiebe model. Thus, it is found that the predictive model adopted in this study consistently represents the combustion phenomenon.
Similarly to the fraction of mass burned, there is satisfactory agreement among the analyzed models with respect to the logP–logV diagram, which provides a clearer view of the processes that make up the engine's thermodynamic cycle. It is noted that the pressure results obtained by the developed model show good agreement throughout all stages of the cycle.

3.2. Parametric study of the oxygen-enriched combustion model

The simulations were carried out using biogas as the fuel, with a fixed composition of 60% CH_4 and 40% CO_2. The effects of enriching the engine's intake air on biogas combustion and performance parameters were evaluated, for a variation in oxygen concentration ranging from 21% to 30% oxygen by volume. In addition to the oxygen concentration in the air, the simulations considered different values for ignition timing, rotational speed, compression ratio and intake pressure. The range of variation for these parameters is shown in Table 2

Table 2: Range of variables.

Parameter	Minimum	Maximum
Ignition advance [°CA]	-40	-5
Engine speed [rpm]	1500	4000
Oxygen percentage [%]	21	30
Compression ratio	12	16
Intake pressure [kPa]	80	115

3.3. Effect of ignition advance

The variation in the start point and, consequently, the end point of the combustion process can be clearly seen from the mass fraction curves shown in Fig 4 (a). It can be observed that the end of the combustion process is progressively delayed as the start point of combustion is postponed. According to [22], due to this progressive delay in the end of combustion, the peak pressure in the cylinder tends to occur later in the expansion stroke, as well as showing a reduction in its magnitude. This argument confirms the consistency of the results obtained for the pressure curves shown in Fig 4 (b).

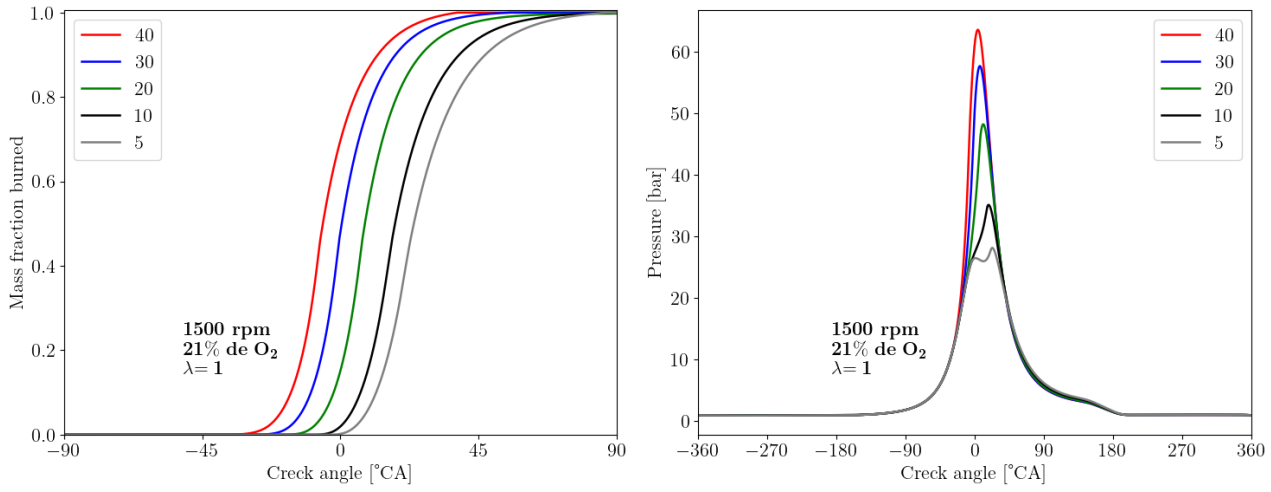

Figure 4: Mass fraction burned and cylinder pressure as a function of ignition timing.

The gradual advance or retardation of the ignition timing affects both the location and magnitude of the peak pressure in the cylinder, enabling the identification of the point at which maximum torque is achieved, known as Maximum Brake Torque (MBT). Figure 5 shows the torque and mean effective pressure (imep) values as a function of ignition advance. It can be seen that maximum torque and imep occur at an ignition advance angle of -30 °CA.

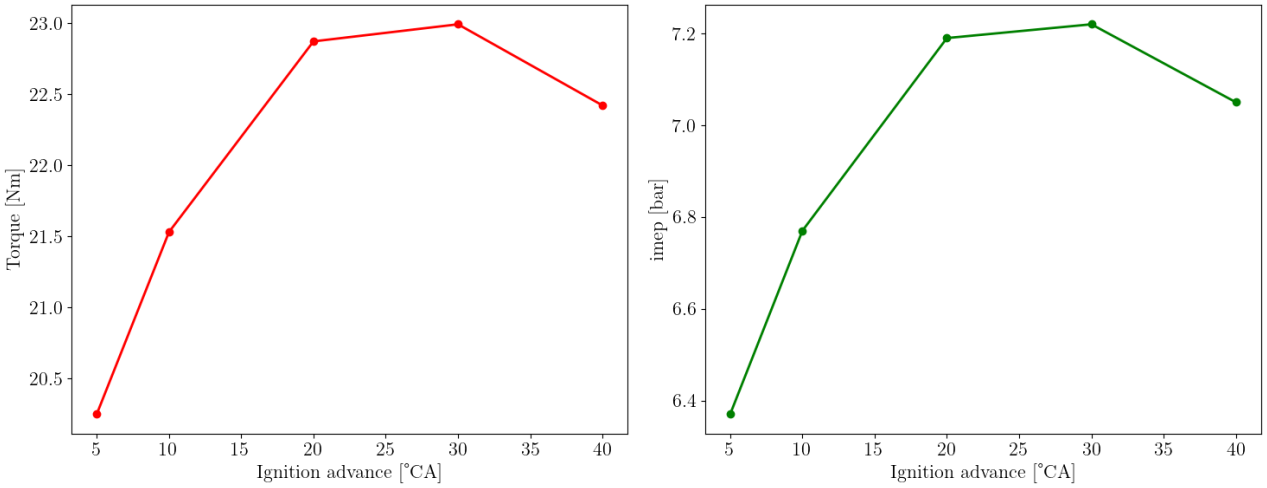

Figure 5: Engine torque and imep as a function of the spark advance.

3.4. The influence of rotational speed and oxygen enrichment

The analysis of the influence of variations in crankshaft rotational speed on the performance of the simulated engine was conducted based on the input data presented in Table 1. In this context, only the rotational speed and the oxygen concentration in the intake air were varied, while the other parameters were kept constant. Furthermore, the ignition advance angle was adjusted to obtain the maximum torque (MBT) for each evaluated operating condition.

The increase in maximum pressure and temperature levels, resulting from higher oxygen concentrations in the intake air leads to an increase in flame velocities, both laminar and turbulent. This effect promotes higher flame front propagation rates and, consequently, reduces the duration of combustion, as shown in the results presented in Fig 6 (a).

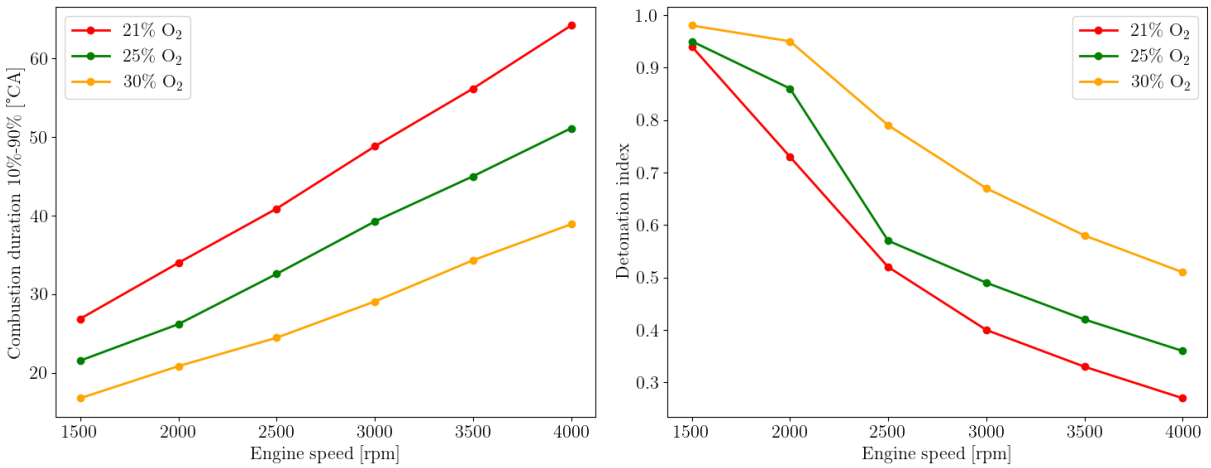

Figure 6: Combustion duration for different oxygen percentages as a function of engine speed.

The detonation index is higher at low engine speeds and at higher oxygen concentrations. This behavior can be attributed to the fact that, at low engine speeds, unburned gases remain exposed to high pressure and temperature levels for a longer period of time. Furthermore, as discussed earlier, enriching the air with O2 results in a more intense combustion process, characterized by higher pressures and temperatures, which promotes the occurrence of detonation.

The results presented in the Fig 7 indicate that torque and power exhibit distinct behaviors in response to changes in rotational speed. However, both show a significant increase due to oxygen enrichment. These results are consistent with the performance characteristics observed in real engines, which exhibit high torque values at low rotation speeds and higher power values at high crankshaft rotational

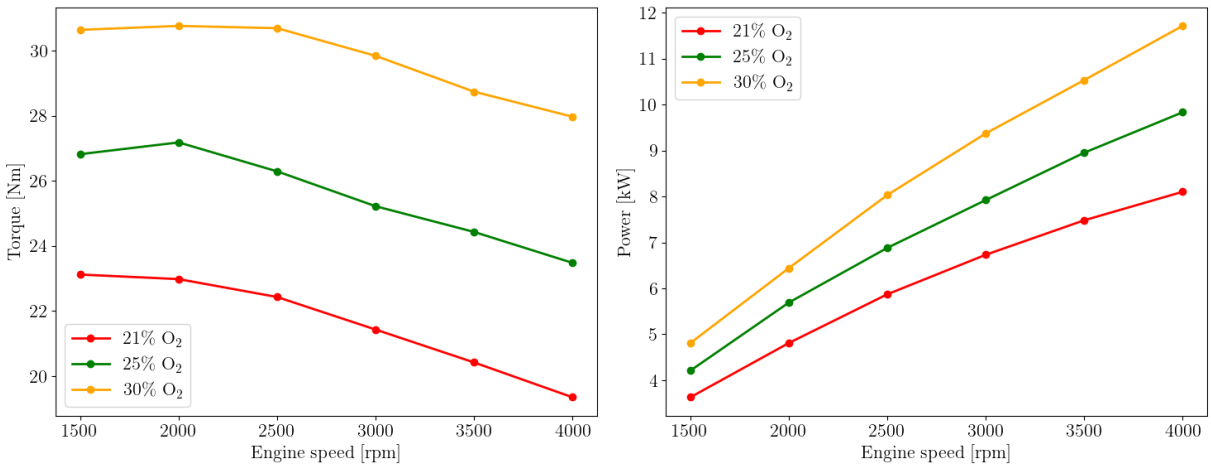

Figure 7: Torque and power as a function of engine speed.

speeds. The increase in O2 concentration reduces the presence of inert gases in the air, helping to mitigate the adverse effects of high CO2 concentration in the biogas. As a result, an increase in pressures during combustion is observed, directly leading to increases in the torque and power generated by the engine.

3.5. Effects of the compression ratio and applied load

Another option for improving the operating characteristics and performance parameters of MCI engines is the use of a turbocharger, which recovers the energy contained in the exhaust gases to increase the pressure of the intake air. In this study, the effect of varying the intake pressure was evaluated to illustrate the impact of using a turbocharger.

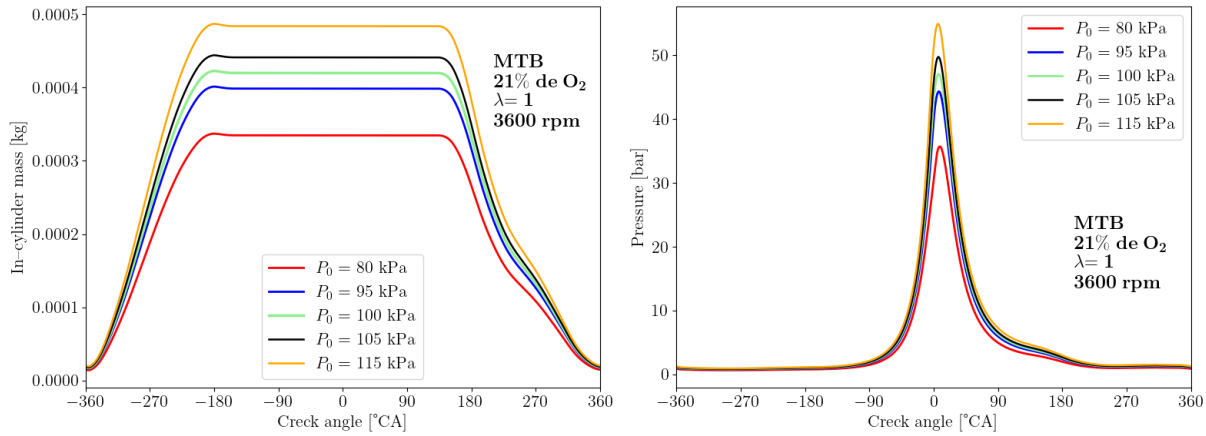

Figure 8: In cylinder trapped mass and cylinder pressure as a funtion of engine speed for 21% oxygen.

It can be seen that both the combustion rate and the pressure values increase as the intake pressure rises. This trend was expected and is consistent with the behaviour observed in real engines, since the pressure gradient between the intake manifold and the combustion chamber intensifies with increasing intake pressure, resulting in a higher mass flow into the cylinder, that is, it promotes greater cylinder filling capacity, as shown in Figs 8 to 10.

The greater the mass of air admitted into the cylinders, the more this directly affects the engine's operating characteristics, as it allows for the use of a greater quantity of fuel and, consequently, the release of a greater amount of chemical energy during the combustion reaction, resulting in significant increases in pressure and in the performance parameters of the simulated engine.

Figure 11 shows the effects of varying intake pressure on volumetric efficiency and specific power. A substantial increase is observed in both parameters, particularly in volumetric efficiency, which shows

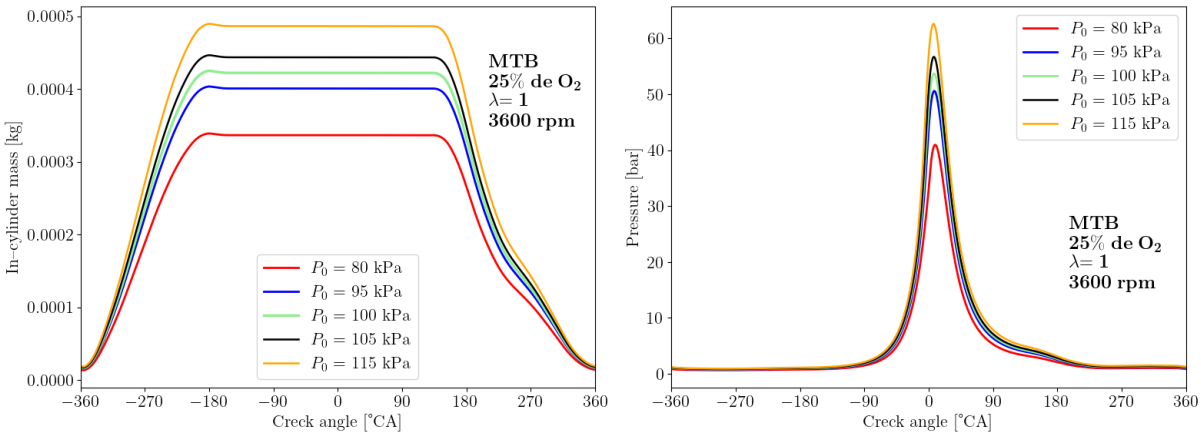

Figure 9: In cylinder trapped mass and cylinder pressure as a funtion of engine speed for 25% oxygen.

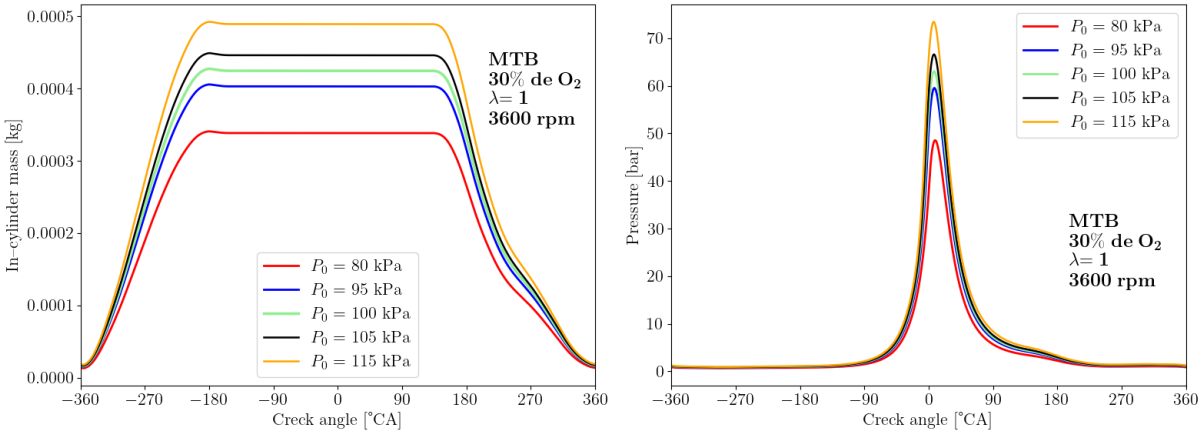

Figure 10: In cylinder trapped mass and cylinder pressure as a funtion of engine speed for 30% oxygen.

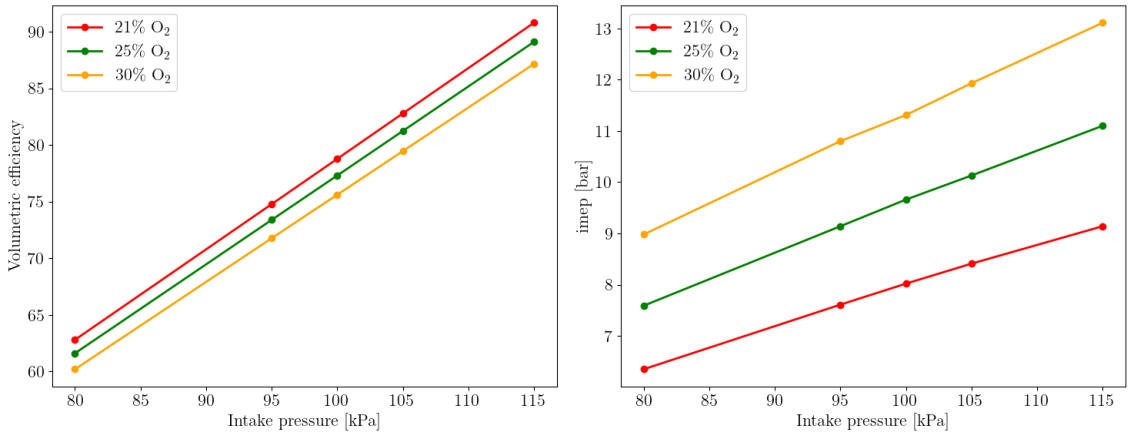

Figure 11: Volumetric efficiency and imep as a function of the intake pressure.

an approximate gain of 44% when comparing the values obtained at maximum and minimum intake pressures. The increase in pressure levels within the cylinder results in greater net work per cycle, which, in turn, has a positive impact on torque, power and imep values.

As shown in Tables 3 and 4, the results indicate that the use of a turbocharger would yield higher performance parameters than those achieved by varying the compression ratio alone. Furthermore, it is observed that increasing the compression ratio makes the engine more susceptible to knocking, since it favors thermodynamic conditions conducive to the development of this phenomenon.

Table 3: Performance parameters as a function of the compression ratio for 30 % de O_2 .

Parameters	12	14	16
Power [kW]	10.78	11.21	11.54
Torque [Nm]	28.61	29.75	30.63
Thermal efficiency [%]	32.60	34.02	35.09
Volumetric efficiency [%]	71.77	71.55	71.30
imep [bar]	8.98	9.34	9.61
Detonation index [-]	0.55	0.86	1.25

Table 4: Performance parameters as a function of intake pressure for 30 % de O_2.

Parameters	80	95	100	105	115
Power [kW]	8.98	10.78	11.31	11.93	13.11
Torque [Nm]	23.83	28.61	30.02	31.66	34.69
Thermal efficiency [%]	32.43	32.60	32.46	32.57	32.58
Volumetric efficiency [%]	60.20	71.77	75.61	79.46	87.16
imep [bar]	7.49	8.98	9.43	9.95	10.93
Detonation index [-]	0.38	0.55	0.61	0.68	0.81

4. Conclusions

The two-zone quasi-dimensional model, consisting of a phenomenological model for describing the thermodynamic cycle and a turbulent combustion model for representing the combustion process, proved to be highly suitable for the computational simulation of an MCI operating on biogas or ethanol, since, when the results were evaluated in comparison with those obtained from engine simulation models found in the literature, the results showed high agreement when the same input data were used for simulation.

Oxygen enrichment proved to be an effective alternative for improving the performance parameters of engines operating with biogas, as it mitigates the effects of the high concentration of inert gases present in both air and biogas (N_2 and CO_2). As a result, a larger fraction of the chemical energy released during combustion can be converted into net work. This phenomenon is associated with the increase in in-cylinder pressure levels. Consequently, significant gains are observed in imep, torque, and engine power output.

In conjunction with oxygen enrichment of the intake air, increasing the compression ratio proved to be a promising strategy for improving the performance characteristics of the analyzed engine. However, it was observed that raising this parameter leads to a significant increase in the knock index, due to the high pressures and temperatures reached during the combustion process, which limits the benefits of this modification.

As a more effective alternative to be adopted alongside oxygen enrichment, the application of a turbocharger proved to be more advantageous. This solution, by increasing the intake pressure and, consequently, the amount of air–fuel mixture inducted into the engine, promotes more substantial gains in performance parameters, while also allowing engine operation under conditions less prone to knock occurrence.

Furthermore, the use of a turbocharger enables a more efficient utilization of the increased exhaust gas temperatures resulting from oxygen enrichment, contributing to an additional improvement in the overall system performance.

Nomenclature

Latin

A surface area, m^2

A_f Flame front area, m^2

A_p piston area, m^2

A_{iv} maximum opening area of the intake valve, m^2

cp specific heat, J(kgK)

H_{comb} extensive heat of combustion, kJ

h_{comb} intensive combustion enthalpy, kJ/kg

h^{HT} heat transfer coefficient, (W $(\mathrm{m}^2\mathrm{K})^{-1}$)

l_t characteristic length scale of turbulence, m

L piston stroke, m

L_{iv} maximum lift of the intake valve, m

m mass, kg

m_b burnt mass, kg

m_e dragged mass, kg

$\dot{m}_b$ burn rate, $(\mathrm{kg(s)})^{-1}$)

$\dot{m}_e$ drag rate, $(\mathrm{kg(s)})^{-1}$)

m_{comb} fuel mass, kg

P Pressure, $(\mathrm{N(m}^2))^{-1}$)

Q heat, J

R specific gas constant, $(\mathrm{J(kgK)})^{-1}$)

R_f front flame radius, m

S_l laminar flame velocity, $(\mathrm{m(s)})^{-1}$)

T Temperature, K

x_b Fraction of mass burned

Greek symbols

η efficiency

θ cranck angle, degrees

ω engine angular speed, $(\mathrm{rad(s)})^{-1}$)

τ characteristic burning time (s)

ρ density $(\mathrm{kg(m}^3))^{-1}$)

λ theoretical air coefficient

Subscripts and superscripts

comb combustion

b burnt

u unburnt

e entrainment

0 reference state

iv intake valve

i inlet

l laminar

References

[1] Reitz, R. D., Ogawa, H., Payri, R., Fansler, T., Kokjohn, S., Moriyoshi, Y., Agarwal, A., Arcoumanis, D., Assanis, D., Bae, C. et al. *Ijer editorial: The future of the internal combustion engine. International Journal of Engine Research,* v. 21, n. 1, p. 3–10, 2020.

[2] International Energy Agency. *World Energy Outlook 2023* Available at: `https://www.iea.org/reports/worldenergy-outlook-2023` [accessed 04.4.2024].

[3] Akerlind, I. B.; Bastani, P.; Berry, I.; Bhatt, K.; Chao, A.; Chow, E.; Karplus, V.; Keither, D.; Khusid, M. N. E.; Zoepf, S. *On the road toward 2050. J. Heywood J. and Don M eds., Massachusetts Institute of Technology,*. Cambridge, UK: Cambridge; 2015.

[4] Sun, Q.; Li, H.; Yan, J.; Liu, L.; Yu, Z.; Yu, X., *Selection of appropriate biogas upgrading technology-a review of biogas cleaning, upgrading and utilisation*. Renewable and sustainable energy reviews, v. 51, p. 521–532, 2015.

[5] Scarlat, N.; Dallemand, J.-F.; Fahl, F., *Biogas: Developments and perspectives in europe*. Renewable energy, v. 129, p. 457–472, 2018.

[6] Crookes, R., *Comparative bio-fuel performance in internal combustion engines.* Biomass and Bioenergy, v. 30, n. 5, p. 461–468, 2006.

[7] Porpatham, E.; Ramesh, A.; Nagalingam, B., *Experimental studies on the effects of enhancing the concentration of oxygen in the inducted charge of a biogas fuelled spark ignition engine.* Energy, v. 142, p. 303–312, 2018.

[8] Eckl, F.; Moita, A.; Castro, R.; Neto, R. C., *Valorization of the by-product oxygen from green hydrogen production: A review.* Applied Energy, v. 378, p. 124817, 2025.

[9] Cacua, K.; Amell, A.; Cadavid, F., *Effects of oxygen enriched air on the operation and performance of a diesel-biogas dual fuel engine.* Biomass and bioenergy, v. 45, p. 159–167, 2012.

[10] Rufino, C. H. *Conceptual study of an internal combustion engine with adjustable cubic capacity and compression ratio [thesis]* Campinas, Brazil: University of Campinas; 2020.

[11] Hohenberg, G. F., *Advanced approaches for heat transfer calculations.* SAE Transactions, p. 2788–2806, 1979.

[12] Nishiwaki, K.; Shimamoto, Y.; Miyake, K., *Average heat transfer coefficients on a cylinder wall in the intake and exhaust processes of motoring test.* Bulletin of JSME, v. 22, n. 174, p. 1796–1809, 1979.

[13] Perini, F.; Paltrinieri, F.; Mattarelli, E., *A quasi-dimensional combustion model for performance and emissions of si engines running on hydrogen–methane blends.* International journal of hydrogen energy, v. 35, n. 10, p. 4687–4701, 2010.

[14] Cró, N. P. R. *Modelo para simulação computacional do ciclo termodinâmico de motores de combustão interna com ignição por centelha. [dissertation]* Campinas, Brazil: University of Campinas; 2014.

[15] Mattos, A. P. *Estudo do desempenho de um motor turbo alimentado a etanol empregando EGR para redução de emissões de NOx e controle de detonação. [thesis]* Campinas, Brazil: University of Campinas; 2018.

[16] Annand, W., *Heat transfer in the cylinders of reciprocating internal combustion engines.* Proceedings of the Institution of Mechanical Engineers, v. 177, n. 1, p. 973–996, 1963.

[17] Gallo, W. L. R., *Análise exergética de motores a gasolina e a álcool. [thesis]* Campinas, Brazil: University of Campinas; 1990.

[18] Blizard, Norman C and Keck, James C., *Experimental and theoretical investigation of turbulent burning model for internal combustion engines.* Automotive engineering congress and exposition, SAE Technical Paper, 1974.

[19] Rakopoulos, C. and Michos, C., *Quasi-dimensional, multi-zone combustion modelling of turbulent entrainment and flame stretch for a spark ignition engine fuelled with hydrogen-enriched biogas.* International journal of vehicle design, v. 49, n. 1-3, p. 3–51, 2009.

[20] Gatowski, J. A.; Heywood, J. B.; Deleplace, C., *Flame photographs in a spark-ignition engine.* Combustion and flame, v. 56, n. 1, p. 71–81, 1984.

[21] Bayraktar, H., *Theoretical investigation of flame propagation process in an si engine running on gasoline–ethanol blends.* Renewable energy, v. 32, n. 5, p. 758–771, 2007.

[22] Heywood, J. B., *Internal combustion engine fundamentals.* Cambridge, McGraw-Hill, 1988.

[23] Beretta, G. P.; Rashidi, M.; Keck, J., *Turbulent flame propagation and combustion in spark ignition engines.* Combustion and flame, v. 52, p. 217–245, 1983.

[24] Medina, A.; Curto-Risso, P. L.; Hernández, A. C.; Guzmán-Vargas, L.; Angulo-Brown, F.;

Sen, A. K., *Quasi-dimensional simulation of spark ignition engines.* Thermodynamic Optimization to Cyclic Variability; Springer: London, UK, 2014.

[25] Smith, G. P.; Golden, D. M.; Frenklach, M.; Moriarty, N. W.; Eiteneer, B.; Goldenberg, M.; Bowman, C. T.; Hanson, R. K.; Song, S.; Gardiner, W. C.; Lissianski, V. V.; Qin, Z., *GRI-MECH 3.0* Available at: :https://www.me.berkeley.edu/gri_mech/ [accessed 08.7.2024].

[26] Levenberg, K., *A method for the solution of certain non-linear problems in least squares.* Quarterly of applied mathematics, v. 2, n. 2, p. 164–168, 1944.

[27] Marinov, N. M., *A detailed chemical kinetic model for high temperature ethanol oxidation.* International journal of chemical kinetics, v. 31, n. 3, p. 183–220, 1999.